HYDROLOGICAL PROCESSES
Hydrol. Process. **18**, 757–776 (2004)
Published online in Wiley InterScience (www.interscience.wiley.com). DOI: 10.1002/hyp.1365

Distributed simulations of landslides for different rainfall conditions

Amod S. Dhakal[1]* and Roy C. Sidle[2]

[1] *Department of Forest Resources Management, University of British Columbia, 2nd Floor, Forest Sciences Centre, 2424 Main Mall, Vancouver, BC V6T 1Z4, Canada*

[2] *Slope Conservation Section, Geohazards Division, Disaster Prevention Research Institute, Kyoto University, Gokasho, Uji, Kyoto 611-0011, Japan*

Abstract:

A physically based distributed slope stability model is described that utilizes a combined surface–subsurface kinematic wave module to assess groundwater fluctuations related to slope stability. A total of 82 major rainstorms from 1972 to 1990 in Carnation Creek, British Columbia, were examined to determine the influence of different characteristics of rainstorms (such as mean and maximum hourly intensity, duration, and rainfall amount) on the slope stability. These rainstorms vary in mean intensity from 1·6 to 11·2 mm h^{-1}, storm duration from 11 to 93 h, and maximum hourly intensity from 3·4 to 35 mm h^{-1}. Four synthetic 'uniform intensity' rainstorms were also tested against real storms to assess the effect of short-term hourly rainfall intensity peaks on landslide occurrence. Altogether, 602 simulations were conducted. The combined influence of mean and maximum hourly intensity, duration, and total rainfall amount of rainstorms were important in generating landslides. The temporal distribution of short-term intensity also influenced the landslide occurrence. When saturated hydraulic conductivity of the soil was lowered or soil depth was raised, most rainstorms produced larger numbers of landslides. For the most part, actual rainstorms produced less stable conditions than their synthetic 'uniform intensity' counterparts. For all landslide-producing storms, slope failure usually occurred after some threshold of cumulative rainfall and maximum hourly rainfall intensity. These simulations provide insights into the distributed behaviour of landslide occurrence during large rainstorms with varying characteristics. Copyright © 2004 John Wiley & Sons, Ltd.

KEY WORDS slope stability; groundwater; rainstorms; short-term rainfall intensity; modelling; safety factor; soil depth; hydraulic conductivity

INTRODUCTION

Shallow, rapid landslides typically occur on steep slopes and are often triggered by individual rainstorm events (O'Loughlin *et al*., 1982; Sidle and Swanston, 1982; Tsukamoto *et al*., 1982). Rainstorm characteristics that have been empirically related to shallow groundwater response and associated landslide occurrence include storm mean and maximum hourly intensity, storm duration, rainfall amount, and antecedent rainfall (Caine, 1980; Sidle and Swanston, 1982; Sidle 1984a, 1986; Canuti *et al*., 1985; Wieczorek, 1987; Capecchi and Focardi, 1988; Dhakal, 1995; Finlay *et al*., 1997). During such major rainstorms the pore water pressure builds up in the soil mantle, usually just above the lithic contact or other hydrologic impeding layer (e.g. Onda *et al*., 1992).

The development of empirical relationships between storm characteristics and landslide occurrence has prompted the establishment of threshold rainfall values for landslide hazard assessment, prediction, and warning systems (Keefer *et al*., 1987; Kim *et al*., 1992; Larsen and Simon, 1993; Wieczorek, 1996; d'Orsi *et al*., 1997). Wilson (1997) proposed a simple relationship for regional storm thresholds that triggered

* Correspondence to: Amod S. Dhakal, Department of Forest Resources Management, University of British Columbia, 2nd Floor, Forest Sciences Centre, 2424 Main Mall, Vancouver, BC V6T 1Z4, Canada. E-mail: dhakal@interchange.ubc.ca

Received 27 July 2001
Accepted 10 September 2002

debris flows in the Pacific Northwest based on peak 24 h rainfall versus rainy-day normal values (mean annual precipitation divided by the number of rainfall days). Other studies have attempted to define relationships between storm attributes and landslide/debris flow frequency through the development of rainfall threshold curves, such as for California (Cannon and Ellen, 1985; Keefer *et al*., 1987; Wieczorek, 1987; Johnson and Sitar, 1990), Sri Lanka (Bhandari and Virajh Dias, 1995), and Hong Kong (Kay and Chen, 1995).

In addition to climatic factors, the generation and subsequent dissipation of pore water pressure in surficial soils as a result of rainfall is also governed by the site characteristics, such as hillslope morphology, upslope catchment area, and soil properties (Jackson and Cundy, 1992; Montgomery and Dietrich, 1994; Tarboton, 1997). Additionally, slope geometry affects pore water pressure accretion, especially in highly divergent or convergent terrain (Sidle *et al*., 1985; Jackson and Cundy, 1992; Montgomery and Dietrich, 1994). Preferential flow through discontinuous networks of soil macropores and subsurface pipes is believed to cause a rapid rise in pore water pressure during rainstorms (Pierson, 1983; Sidle, 1984a; Tsukamoto and Ohta, 1988).

Generally, field investigations have shown a common hydrologic sequence for initiation of shallow landslides that involves wet antecedent conditions followed by a prolonged period of rainfall with a burst of high intensity (e.g. Sidle and Swanston, 1982; Larsen and Simon, 1993). The wet antecedent conditions provide the necessary soil moisture to promote a perched water table in unstable sites; the prolonged rainfall gradually builds up pore water pressures; and the high-intensity burst causes pore water pressure to increase rapidly to a threshold that initiates slope failure. Other studies showed that shorter duration rainfall events with very high intensities triggered landslides (Croft and Marston, 1950; Selby, 1976). These findings confirm that shallow landslides initiate during the individual rainstorm events and are highly influenced by the pattern of rainfall, characteristics of rainstorms, and topographic and soil characteristics of the site (Jackson, 1966; Haruyama, 1974; Ekanayake and Phillips, 1999). Only a few studies (e.g. Cannon and Ellen, 1985; Larsen and Simon, 1993; Finlay *et al*., 1997) have clarified in detail the effect of specific rainstorm characteristics on landslide occurrence. In spite of these investigations, the influence of the importance of short-term rainfall intensity peaks in landslide occurrence remains unclear.

The application of results from rainfall–landslide studies at the drainage-basin scale presents a particular challenge because the location of failure depends on the temporal variation of ground water table during rainstorms, which is controlled by the distributed properties of site variables such as topography and soil. The specification of location makes the problem complex compared with most runoff and erosion studies, which only require evaluation of fluxes at the outlets of basins. The distributed slope stability model predicts the pore water pressure necessary to destabilize a slope during a rainstorm. Hence, the application of a distributed, physically based slope stability model that incorporates spatial heterogeneity at the basin scale allows us to examine the influence of different rainstorm characteristics on landslide occurrence.

A PC-based integrated dynamic slope stability model (IDSSM) developed within a C++ coding environment, which is an extensively revised version of an earlier distributed slope stability model (dSLAM; Wu and Sidle, 1995), was used to examine the influence of different rainstorm characteristics on landslide occurrence. IDSSM integrates a geographical information system (GIS) with topographic, distributed hydrologic and vegetation modules to assess the slope stability. The event simulation that uses a particular rainstorm to evaluate spatial distribution of safety factor is one of the simulation scenarios of the model. The objectives of this study utilizing IDSSM are: (1) to examine the influence of different rainstorm characteristics, such as storm mean and maximum hourly intensity, duration, and rainfall amount on landslide occurrence; (2) to examine the influence of temporal distribution of short-term intensities of rainstorms on landslide occurrence; and (3) to evaluate the interaction of rainstorm characteristics and soil properties (e.g. hydraulic conductivity and soil depth) on landslide occurrence. Major rainstorms (with varying characteristics) during the period from 1972 to 1990 in Carnation Creek watershed, Vancouver Island, British Columbia, were used in this analysis.

THE STUDY AREA

The study area is a sub-watershed of Carnation Creek watershed (9·5 km^2) located on the west coast of Vancouver Island (48°54′N, 125°01′W), British Columbia (Figure 1). Carnation Creek empties into Numnkanus Bay of Trevor Channel, part of Berkeley Sound on the west coast of Vancouver Island. The Carnation Creek watershed is the continual focus of numerous studies, primarily including the effects of forest management on the terrestrial and aquatic ecosystems. Carnation Creek lies within the Coastal Western Hemlock Biogeoclimatic Zone (Krajina, 1969), where the forest is mostly comprised of mature western hemlock (*Tsuga heterophylla*), amabilis fir (*Abies amabilis*), and varying amounts of western red cedar (*Thuja plicata*), Douglas fir (*Pseudotsuga menziesii*) and other species (Oswald, 1974). Mean temperatures during July–August and December–January are about 16 °C and 3 °C respectively. The bedrock is composed of Jurassic volcanics of the Bonanza group and consists mainly of basaltic to rhyolitic lava, tuff breccia, and graywacke (Eastwood, 1975; Fuller, 1977).

The study area (Figure 1) comprises tributary basin H and part of the main creek drainage (total of 0·57 km^2), and features quite rugged terrain with steep slopes; elevation ranges from 150 to 290 m. Soils are predominantly coarse-textured colluvium derived from volcanic rocks and classified as orthic ferro-humic podzols (Agriculture Canada Expert Committee on Soil Survey Committee, 1987). Soil depth is shallow, with an average depth of about 100 cm (Hetherington, 1998). Soils in the study area remain moist the year round (Hetherington, 1998). These soils are also highly permeable to water. During the winter, a subsurface water table develops on the slopes and is sustained by the frequent rains. This water table responds rapidly during rainstorms, rising and falling in concert with variations in rainfall intensity (Hetherington, 1982). Owing to the bedrock geology and high percolation rates, the watershed exhibits a very flashy storm runoff pattern. Streamflow conforms closely to rainfall (Hetherington, 1982). Approximately 80% of the study area

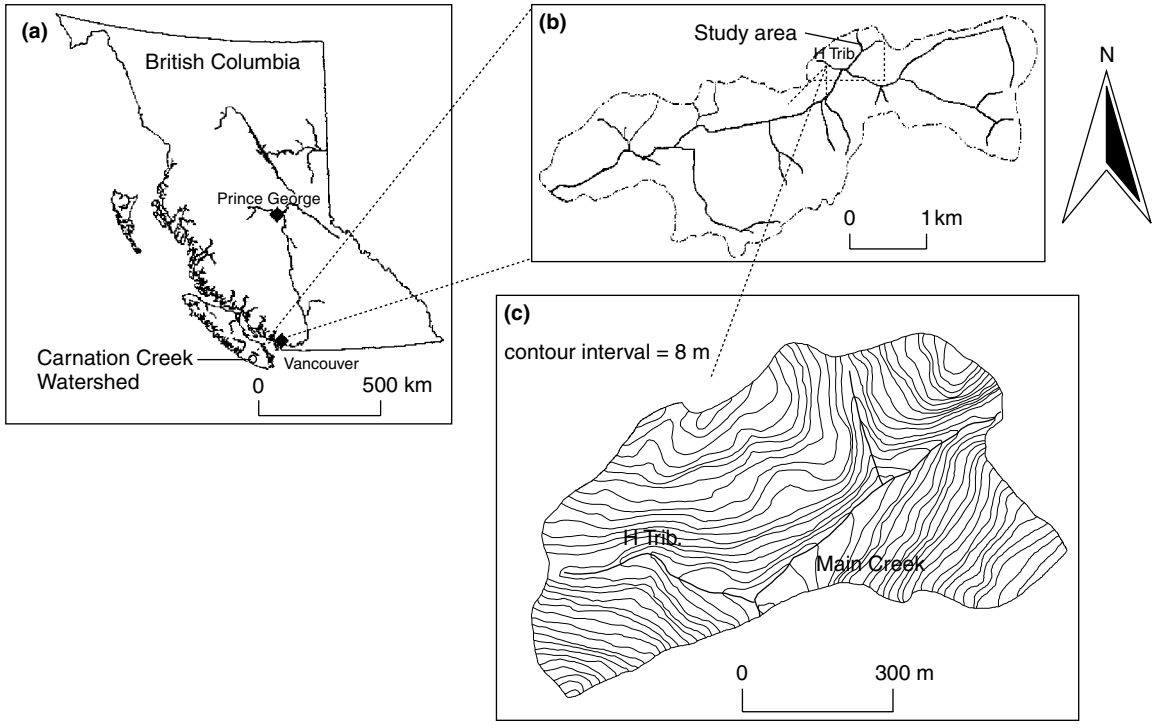

Figure 1. The location of the study area Carnation Creek sub-watershed, Vancouver Island, British Columbia. (a) Location of the Carnation Creek in British Columbia, (b) Carnation Creek Watershed, and (c) the study area; sub-watershed of Carnation Creek watershed

was clear-cut logged from 1977 to 1978 and 11% was clear-cut logged from 1979 to 1980 (Hartman and Scrivener, 1990).

OUTLINE OF IDSSM AND METHODS OF ANALYSIS

The two sub-models of IDSSM used in this study comprise: (1) a topographic analysis model for integrated slope stability (TopoTube); and (2) dSLAM II. TopoTube, developed in the C++ environment, partitions the drainage basin into vector-based stream tube elements and calculates different attributes using contours generated in the ARC/INFO GIS based on concepts of the TAPES-C model (Moore *et al*., 1988). Streamtubes of irregular size are defined by adjacent contours and streamlines; these form the basic modelling unit or element. dSLAM II, developed for the PC environment using C++ coding, is an extensively modified and upgraded version of dSLAM that was developed for the Unix environment using C code (Wu and Sidle, 1995).

The slope stability analysis incorporates a planar infinite slope analysis module, a continuous temporal change root cohesion and vegetation surcharge module, and a kinematic wave groundwater module. The model assesses safety factor for potential shallow translational landslides that overlie a lithic contact. Groundwater is assumed to flow parallel to the slope surface. The net rooting strength of a forested hillslope subject to harvesting is determined by the regeneration rate of new vegetation after harvesting (represented by a sigmoid curve), and the rate of root strength deterioration of harvested trees (represented by a negative exponential curve) (Sidle, 1991, 1992). The rates of these simultaneous functions determine the temporal changes in net rooting strength for different harvesting and silvicultural scenarios (Sidle, 1991, 1992). Vegetation surcharge is assumed to increase according to the sigmoid function (Sidle, 1992).

Following Moore and Grayson (1991), the combined surface–subsurface kinematic wave modelling approach was adopted in the groundwater module (Takasao and Shiiba, 1988). It is assumed that the infiltration capacity of soil is always in excess of the rainfall intensity; thus, Hortonian overland flow is ignored and only saturated overland flow is considered (Dunne, 1978). The one-dimensional form of the continuity equation that is applied to each element can be written as

$$\frac{\partial A}{\partial t} + \frac{\partial Q}{\partial x} = \frac{iA_e}{\Delta x_e} \tag{1}$$

where $A(m^2)$ is the apparent cross-sectional flow area, i (m s^{-1}) is the rainfall intensity, Q (m^3 s^{-1}) is the discharge per unit width, A_e (m^2) is the plan area of the element, and ΔX_e(m) is the flow distance along a stream line through the element. The 'apparent' cross-sectional flow areas for the cases of subsurface flow only and of combined subsurface and saturation overland flow are given in Equations (2) and (3) respectively. Similarly, the kinematic forms of the momentum equations for subsurface flow only (Equation (4)) and for combined subsurface flow and saturation overland flow (Equation (5)) can be expressed in terms of the Darcy and Manning equations respectively.

$$A = \omega\varepsilon h \qquad \text{for} \qquad 0 \le A < \omega\varepsilon D \text{ or} 0 \le h < D \tag{2}$$

$$A = \omega\varepsilon D + A_c \qquad \text{for} \qquad A > \omega\varepsilon D \tag{3}$$

$$Q = K(A/\varepsilon)\sin\beta = \omega hK\sin\beta \qquad \text{for} \qquad 0 \le A \ge \omega\varepsilon D,\ 0 \le h \le D \tag{4}$$

$$Q = \omega DK\sin\beta + \alpha {A_c}^m \qquad \text{for} \qquad A > \omega\varepsilon D \tag{5}$$

where ω (m) is the width of the element orthogonal to the streamlines, ε is the drainable porosity, D (m) is vertical soil depth and h(m) is the depth of flow above the impermeable layer. $A_c = \omega(h - D)$ for broad sheet flow, where $(h - D)$ is overland flow depth $(h > D)$, and A_c is the channel cross-sectional area when flow concentrates in rills or in a defined channel. K (m s^{-1}) is the effective hydraulic conductivity, β (degrees) is the local slope, $\alpha = n^{-1}\omega^{-2/3}\tan^{1/2}\beta$ and $m = 5/3$ for broad sheet overland flow, $\alpha = n^{-1}\zeta^{2/3}\tan^{1/2}\beta$ and

$m = 4/3$ for channelized flow, n is Manning's roughness coefficient, and ζ is the coefficient in the assumed relationship between hydraulic radius R (m) and the cross-sectional area of a channel, $R = \zeta A_c^{1/2}$ (Moore and Burch, 1986).

Smith's (1980) general algorithm for the kinematic wave flow equation is used to route the subsurface and surface flows between elements. For each element, the streamlines define no-flow boundaries, the upper contour is an inflow boundary, and the lower contour outflow boundary is the computational 'node' (Grayson *et al*., 1992). The temporal sequence of rainfall determines the simulation time step.

For water routing, the method proposed by Moore and Grayson (1991) was used. In non-channelized elements, the tributary outflow cross-sectional areas of the upslope elements are summed up to provide the inflow cross-sectional area to the downslope element. In channelized elements, only the upslope tributary element with the dominant discharge contributes directly to inflow; other elements become lateral inflow to the channel. Channels are defined using the threshold upslope area criterion (Band, 1986). Water in channel elements is considered as channel flow and the elements are excluded from the slope stability analysis.

The calculated h values for each time step are then incorporated into the infinite slope model to determine the safety factor of elements. An average of the h values obtained at upslope and downslope widths of an element is used in simulations for that element. When the calculated safety factor at any time step becomes unity or less for a given element, the safety factor is not calculated for subsequent time steps for that element. The minimum safety factor, the time step corresponding to this minimum and the groundwater saturation level for a rainstorm are stored as output for all elements.

Data acquisition

A vector digital elevation model was generated by digitizing contours of a 1 : 5000 topographic map (contour interval 8 m; Ministry of Forests, 1991), and was used as input for the TopoTube sub-model. TopoTube directly accepts the outputs of contour information created in ArcInfo as inputs. The output files of TopoTube consist of: (1) an ASCII file representing stream tubes; and (2) an ASCII file representing topographic attributes of all the stream tube elements. The ASCII output file of stream tubes was imported into ArcInfo to create a stream tubes network (Figure 2), which was later used for modelling and other data preparation for dSLAM II. The vegetation layer was created from a vegetation map (1 : 15 000) of the area; vegetation was divided into five classes. The soil map (1 : 15 000), containing two soil-mapping units in the study area, was digitized. Clear-cut harvested blocks were also digitized from the harvesting boundary lines depicted on a 1 : 15 000 map. The stream tubes network layer was overlaid with these three layers in order to extract a relational database for each stream tube element.

Two different engineering properties of the soil used for the simulation are listed in Table I. The value of soil cohesion was set to 2·8 kPa, based on values observed for similar soils in different areas (Schroeder and Alto, 1983; Sidle, 1984b). For many soils of colluvial material, Carson and Kirkby (1972) gave values of internal angle of friction between 39° and 47°. A mean value of 43° was used in this study. Unit weights of soils were taken from Graeme (1985), who measured the values in Carnation Creek adjacent to the study area. Soil depth in the study area varies from 85 to 178 cm (Fannin *et al*., 2000); an average value of 1 m was used in this study. Fannin *et al*. (2000) gave estimated ranges of hydraulic conductivity in the study area; an average value of $1{\cdot}4 \times 10^{-3}$ m s^{-1} was adopted as saturated hydraulic conductivity K_{sat}. Owing to unavailability of data, the same soil properties were applied to both soil types. A contributing area of 2500 m^2 was considered necessary to initiate a perennial channel. Montgomery and Dietrich (1988) found similar contributing areas for Coos Bay, Oregon, and Wu and Sidle (1995) used the same area for the Cedar Creek basin, also in the Oregon Coast Ranges. The channels were assumed to be parabolic; the depth–width ratio of the channel was assumed to be two, so that the relationship between hydraulic radius and cross-sectional area of the channel was $\zeta = 0{\cdot}364$ (Moore and Burch, 1986).

Table I also shows parameters for root cohesion and surcharge models. Inflection points for root strength and surcharge curves are designated as t_i and t_{st} (in years) respectively; k and n are empirical constants for the

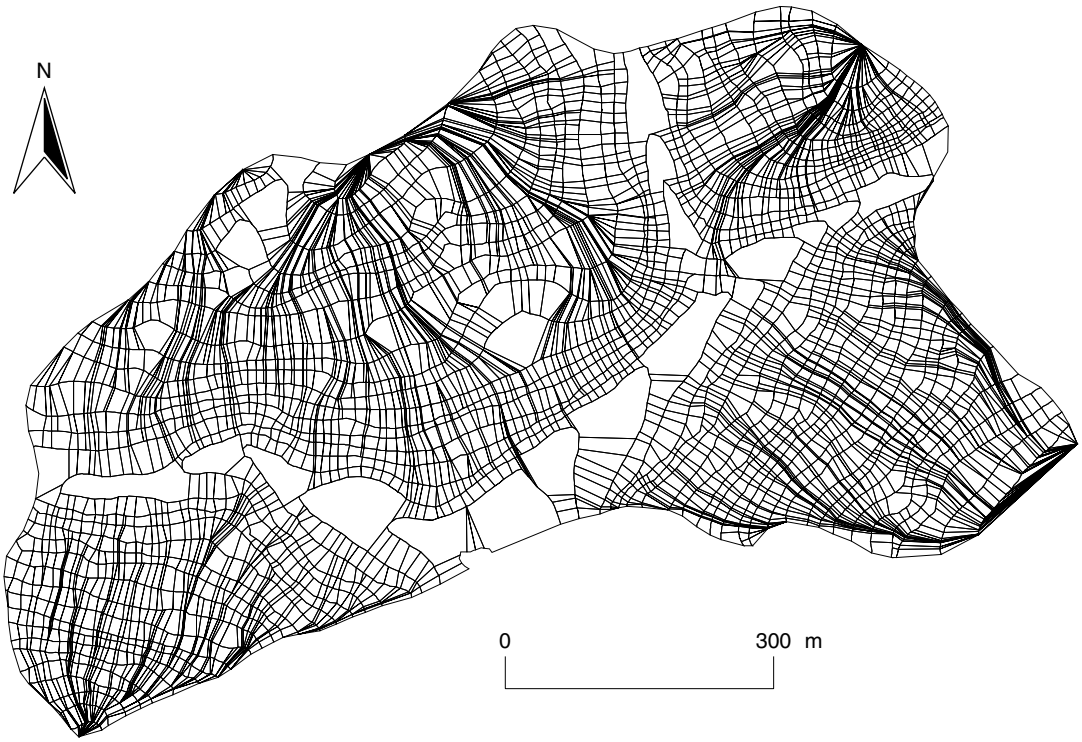

Figure 2. Stream tubes network generated from TopoTube for the Carnation Creek sub-watershed

Table I. Soil engineering properties and vegetation parameters used in the simulations[a]

Soil properties		Vegetation parameters	
C (kPa)	2·8	t_i (years)	25
γ_{sal} (kN m^{-3})	11·3	t_{si} (years)	30
γ_m (kN m^{-3})	13·7	K	0·0958
ϕ	43	n	0·986
K (m s^{-1})	$1{\cdot}4 \times 10^{-3}$	ΔC_{max} (kPa)	6·0
Soil depth (m)	1·0	W_{max} (kPa)	2·5
		R_l	0·9
		R_{sl}	0·99

[a] Soil engineering properties are based on Schroeder and Alto (1983), Sidle (1984b), Carson (1972), Graeme (1985), Fannin *et al*. (2000); and vegetation parameters are based on Sidle (1991, 1992). See text for the explanation of different vegetation parameters.

root decay curve; ΔC_{max} and W_{max} are the maximum potential root cohesion and surcharge for a particular vegetation type respectively; and R_l and R_{Sl} are the scaled root strength and surcharge at times $2t_i$ and $2t_{si}$ (Sidle, 1991). These parameters depend on the vegetation type. Sidle (1991) gave values of these parameters for six vegetation types. Since western hemlock (*T. heterophyla*) is the major vegetation type throughout the study site, the values given by Sidle (1991) for western hemlock–Sitka spruce were adopted. Though the study area was divided into five different vegetation associations, only one set of vegetation parameters was

used because western hemlock is the major species in all five categories. The IDSSM provides a sophisticated environment for long-term modelling of landslides following harvesting and considers the cumulative effects of root strength and vegetation surcharge, topics has been addressed in Dhakal and Sidle (2003).

Precipitation analysis of the study area

Long-term precipitation data from Carnation Creek for the period from 1972 to 1990 were analysed and used for the simulations. Climatic data proximate to Carnation Creek have been recorded at 10 stations either in the watershed or near its perimeter since 1972 (Hartman and Scrivener, 1990). Station H is within the study area and station E is located adjacent to the southeast boundary of the study area. A total of 18 years of hourly precipitation data recorded at these two stations were analysed to determine the characteristics of rainstorms in the area. These data revealed an annual precipitation range from 2300 to 4800 mm, with an average of 3200 mm (Table II). Some 75% of the total rainfall occurred in the fall to winter period (October to March), during which almost 1 in 3 days experienced rain, whereas during the spring to summer period (April to September) only 1 in 5 days experienced rain. High-intensity rainstorms (up to 35 mm h^{-1}) occurred during the fall to winter period. All these scenarios indicate that the fall–winter rainy season is the vulnerable period of erosion and landslide activity in this west-coast region. If rainstorms are defined as periods with >10 mm of total rainfall amount separated by at least 6 h of rainfall less than 1 mm h^{-1}, then the total number of rainstorms in the study area during the 18 year period was 1137; an average of 63 rainstorms per year. Not all of these rainstorms are geomorphically important (Ziemer *et al.*, 1991). Hence, these rainstorms were further divided into four different categories with respect to total rainfall amount based on apparent geomorphic significance. These categories include: <25 mm (least significant); 25–50 mm (less significant); 50–100 mm (moderately significant); and >100 mm (highly significant). Characteristics of these four rainstorm categories are summarized in Table III. Of these rainstorms, 75% are geomorphically least or less significant.

Table II. Characteristics of annual rainfall in the study area during the period 1972–90

Year	Total rainfall (mm)		Rainfall hours		Rainy days		Rainfall intensity (mm h^{-1})				Storm number
	Oct–Mar	Apr–Sep	Oct–Mar	Apr–Sep	Oct–Mar	Apr–Sep	Mean		Hourly Max.		
							Oct–Mar	Apr–Sep	Oct–Mar	Apr–Sep	
1972–73	2289	640	1217	548	108	74	1·9	1·2	21·4	8·0	59
1973–74	3576	910	1712	559	135	70	2·1	1·6	18·4	9·2	82
1974–75	2228	729	1024	347	112	61	2·2	2·1	16·9	11·9	66
1975–76	3710	761	1869	774	140	87	2·0	1·0	22·5	8·1	83
1976–77	2077	788	942	508	89	69	2·2	1·6	13·5	8·0	56
1977–78	2234	1133	1197	725	117	70	1·9	1·6	30·4	7·6	65
1978–79	1702	821	1409	1135	109	89	1·2	0·7	14·1	12·0	51
1979–80	2265	786	1602	948	113	84	1·4	0·8	11·4	21·8	61
1980–81	2413	1097	1718	1532	112	108	1·4	0·7	17·4	11·7	67
1981–82	2522	558	2248	745	125	61	1·1	0·7	14·0	12·4	60
1982–83	3342	687	2333	1072	133	87	1·4	0·6	13·7	9·4	64
1983–84	2535	1019	2192	1400	127	106	1·2	0·7	34·8	7·9	85
1984–85	1779	532	1856	1153	126	102	1·0	0·5	12·6	7·1	44
1985–86	2487	823	2163	1007	146	100	1·1	0·8	19·7	8·6	61
1986–87	2304	780	1686	900	125	73	1·4	0·9	16·2	8·6	57
1987–88	1918	923	1606	1023	108	82	1·2	0·9	16·0	9·1	60
1988–89	2050	531	1998	798	138	73	1·0	0·7	13·7	14·5	62
1989–90	2304	605	1889	811	129	72	1·2	0·7	23·2	14·8	54
Average	2430	785	1703	888	122	82	1·5	1·0	18·3	10·6	63

Table III. Characteristics of rainstorm events in the study area during the period 1972–90

Total rainfall amount (mm)	Total storms 1972–90	Average storms in a year	Mean duration [range] (h)	Rainfall intensity [range] (mm h^{-1})		Mean 24 h antecedent rainfall (mm)	Geomorphic significance
				Mean	Hourly Max		
<25	530	30	10 [1–26]	2·0 [0·6–13·6]	3·9 [1·2–13·6]	10·5	Least
25–50	322	18	15 [4–39]	2·5 [0·9–7·4]	5·5 [2·2–21·2]	10·7	Less
50–100	203	11	27 [8–65]	2·9 [1·2–7·4]	7·4 [2·5–22·5]	10·7	Moderate
>100	82	5	47 [11–93]	3·7 [1·6–11·2]	10·7 [3·4–34·8]	12·9	High

Geomorphically significant rainstorms (moderate and high categories) exhibit a large mean and maximum hourly intensity, and duration. The mean 24 h antecedent rainfall does not vary greatly among the categories. The total rainfall for 7% of these storms is >100 mm (highly significant). A total of 82 rainstorms of this magnitude occurred between 1972 and 1990, an average of five rainstorms per year. Among the 82 rainstorms, 76 occurred during the fall to winter season. For these 82 rainstorms, average storm duration was 47 h, ranging from 11 to 93 h. Mean rainfall intensity ranged from 1·6 to 11·2 mm h^{-1} (average 3·7 mm h^{-1}) and maximum hourly intensity from 3·4 to 34·8 mm h^{-1} (average 10·6 mm h^{-1}). Storm duration was fairly well correlated with mean storm intensity and total storm rainfall, whereas maximum hourly intensity was not correlated with duration and total rainfall.

SIMULATION RESULTS AND DISCUSSION

The 82 most significant rainstorms (total rainfall amount >100 mm) were considered in the slope stability simulations. Rainstorms were numbered chronologically according to the date of occurrence. In order to examine the effect of varying intensities of actual rainstorms on landslide occurrence, four hypothetical storms with uniform hyetographs were also generated. The mean intensity and duration of rainstorms derived from actual storms 67, 62, 30, and 58 were used to generate the four hypothetical 'uniform intensity' rainstorms A, B, C, and D respectively (see Table IV for individual rainstorm characteristics). Hence, the mean intensity and duration of storm A are 6·3 mm h^{-1} and 55 h respectively. Similarly for storms B, C, and D, the mean intensities and durations were 6·3 mm h^{-1} and 41 h, 11·2 mm h^{-1} and 11 h, and 2·9 mm h^{-1} and 93 h respectively.

Slope stability was simulated for these 86 rainstorms at 15 years after timber harvesting, a time when root strength was expected to be near its minimum, contributing a worst-case scenario of landslide occurrence. Each simulation was conducted in 1 h time steps. The soil was assumed to be at field capacity before the storm. Mean intensity and duration of these 86 rainstorms together with Caine's (1980) threshold (line AB) for landslide occurrence are shown in Figure 3. Of these storms, 65 produced only one unstable element (failed element; safety factor $\leq$1); of these 65 storms, 36 were below Caines's threshold. Caine's threshold criterion has been found inapplicable in some cases for landslide occurrence (Church and Miles, 1987). Of these rainstorms, 21 produced two or more unstable elements and all of these storms were above Caine's threshold. The characteristics of these 21 rainstorms are shown in Table IV. In order to differentiate between the degree of importance of these rainstorms in initiating landslides, the rainstorms were ranked primarily based on the number of unstable elements produced by them. When the number of unstable elements was the same for many rainstorms, the number of marginally stable elements (safety factor >1 and <1·2) were used to differentiate the subtle differences in the degree of importance. The rainstorms were ranked equally when they produced the same number of unstable and marginally stable elements.

Storm 67, which had the largest total rainfall, produced six unstable elements and 41 marginally stable elements; it was ranked highest (Table IV). The simulated spatial distribution of safety factor for this storm

Table IV. Results of simulations and characteristics of rainstorms that produced large numbers of unstable (safety factor ≤1) and marginally stable (safety factor >1 and <1·2) elements

Storm no.	Date	TRA (mm)	RD (h)	MRI (mm h^{-1})	MXRI (mm h^{-1})	RS	NUE	NMSE
67	22–25 Feb 1986	349	55	6·3	19·67	1	6	41
62	2–4 Jan 1984	260	41	6·3	34·8	2	6	38
45	25–26 Dec 1980	260	32	8·1	15·4	3	4	35
1	15–17 Dec 1972	219	44	4·5	21·4	4	4	18
80	7–9 Nov 1989	304	51	6·0	23·3	5	3	37
A	—	349	55	6·3	6·3	6	3	33
B	—	260	41	6·3	6·3	7	3	24
44	9–10 Dec 1980	185	29	6·4	17·4	8	3	19
30	13 Nov 1977	123	11	11·2	21·5	9	3	12
64	6–9 Oct 1984	295	66	4·5	12·6	10	2	16
27	11–12 Feb 1977	141	21	6·7	13·5	11	2	15
41	12–14 Dec 1979	196	38	5·2	8·7	12	2	14
58	9–12 Feb 1983	269	93	2·9	10·2	12	2	14
18	2–5 Nov 1975	252	68	3·7	13·1	13	2	13
42	16–17 Dec 1979	165	33	5·0	9·7	14	2	12
70	20–26 Dec 1986	282	86	3·3	11·8	14	2	12
C	—	123	11	11·2	11·2	15	2	11
8	2–3 Feb 1974	189	47	4·0	7·9	15	2	11
11	25–28 Mar 1974	236	72	3·3	6·3	15	2	11
47	30 Oct–1 Nov 1981	160	42	3·8	14·0	15	2	11
73	3–5 Mar 1987	212	60	3·5	14·9	15	2	11

[a] TRA: total rainfall amount; RD: rainfall duration; MRI: mean rainfall intensity; MXRI: maximum hourly rainfall intensity; RS: rank of the storm; NUE: number of unstable elements (safety factor ≤1); NMSE: number of marginally stable elements (safety factor >1 and <1·2).

is shown in Figure 4. Hypothetical 'uniform intensity' storm A with the same mean intensity, duration, and total rainfall amount as storm 67 produced only three unstable elements and was ranked sixth. The storm with the largest maximum hourly rainfall intensity (storm 62) generated six unstable elements and 38 marginally stable elements and was ranked second, whereas 'uniform intensity' storm B with the same mean intensity, duration, and total rainfall amount as storm 62 produced three unstable elements and was ranked seventh. The synthesized, short-duration, 'uniform intensity' storm C produced two unstable elements and was ranked 15th, whereas its real counterpart, storm 30, produced three unstable elements and was ranked ninth. Synthesized long-duration, 'uniform intensity' storm D produced one unstable element and was ranked 21st (not shown in Table IV); its real counterpart, storm 58, generated two unstable elements and was ranked 12th. These indicated the importance of temporal distribution of short-term intensity peaks of real rainstorms over uniform-intensity rainstorms for landslide initiation.

Interestingly, the shortest rainstorm (storm 30; 11 h) produced three unstable elements and was ranked ninth, whereas the longest rainstorm (storm 58; 93 h) produced only two unstable elements and was ranked 12th. The shortest storm had the highest mean rainfall intensity (11·2 mm) of all 82 rainstorms; thus, rainfall intensity appeared to be more important in triggering landslides than either duration or total rainfall amount.

Although the combination of mean intensity and duration of these 21 rainstorms was above Caine's threshold, our findings show that none of the individual rainfall characteristics or the combination of two rainstorm characteristics indicated the degree of potential of storms to trigger landslides. The comparison of four of the most significant rainstorms (storms 67, 62, 45 and 1), which produced four or more unstable elements, reveals variations of mean rainfall intensity from 4·5 to 8·1 mm h^{-1}, of maximum hourly intensity from 15·4 to 34·8 mm h^{-1}, of duration from 32 to 55 h, and of total rainfall amount from 219 to 349 mm. Hence, the simulation results suggest that the degree of importance of rainstorms depends on the combined

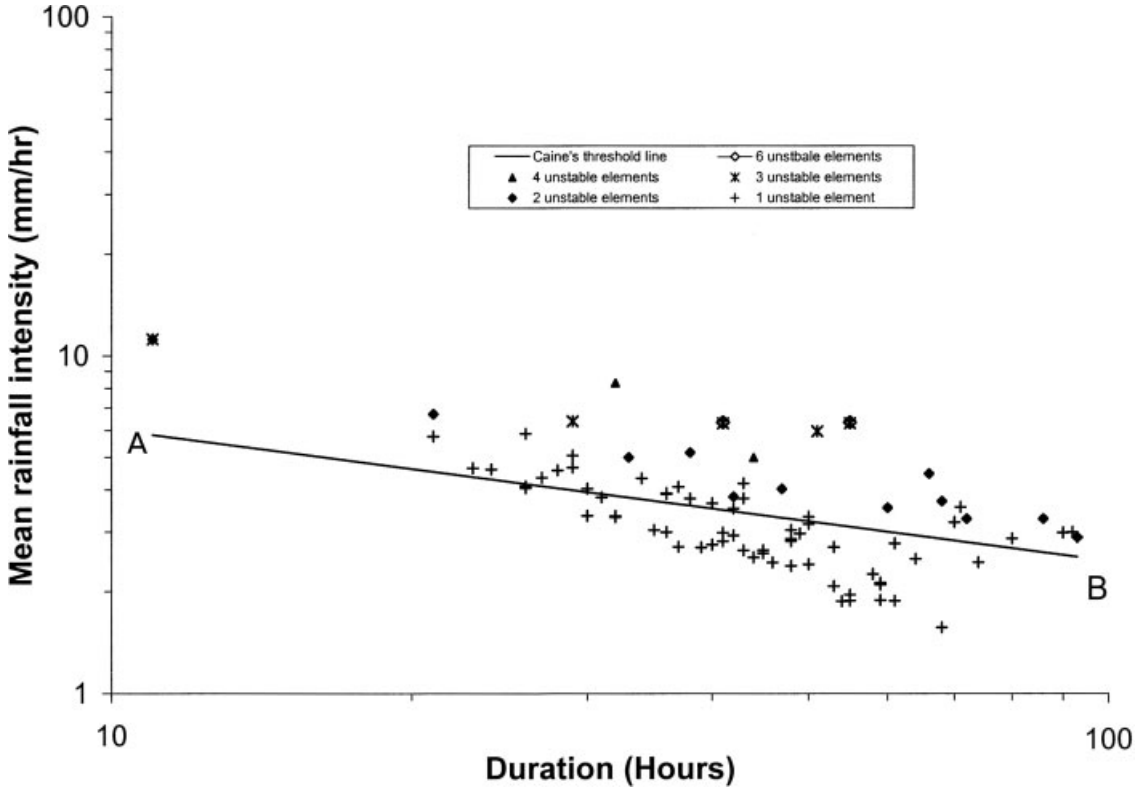

Figure 3. Relationships between mean intensity and duration of 86 rainstorms showing number of unstable (failed) elements produced in the simulations. Line AB represents Caine's threshold

influence of mean and maximum hourly intensity, duration, and total rainfall amount. In addition, the distribution pattern of temporal short-term (hourly) intensity was important for landslide occurrence.

The four characteristics of rainstorms appear inadequate in some cases to depict the distribution pattern of temporal hourly rainfall intensity, and hence the importance of rainstorms. For example, although storm 80 had higher mean and maximum hourly rainfall intensity, duration, and total rainfall amount than storm 1 (see Table IV and Figure 5), storm 1 produced four unstable elements (ranked fourth) and storm 80 produced three unstable elements (ranked fifth). Furthermore, all actual rainstorms produced larger numbers of landslides and were ranked higher than their synthesized 'uniform intensity' counterparts, thus indicating again the importance of short-term rainfall intensity peaks in triggering slope failure. Although the mean intensity and duration may be reasonable parameters to derive broadly applicable thresholds for landslide initiation, these findings suggest that they might fail to represent landslide occurrence in some cases, especially when the temporal distribution pattern of short-term intensity causes unstable conditions. Similarly, mean intensity and duration parameters were insufficient to determine the degree of importance of rainstorms to landsliding occurrence.

Unstable elements and rainstorms

Hyetographs for the six rainstorms (67, 62, 45, 1, 80 and 44, excluding uniform rainstorms) that triggered the most landslides are shown together with the failure time for unstable elements in Figure 5. The time of failure, cumulative rainfall at failure, and rainfall intensity at failure are tabulated for all unstable elements (Table V). Interpreting time of failure for each element in each rainstorm was complicated; however, it appeared that most failures occurred after some threshold cumulative rainfall and maximum hourly rainfall intensity. This

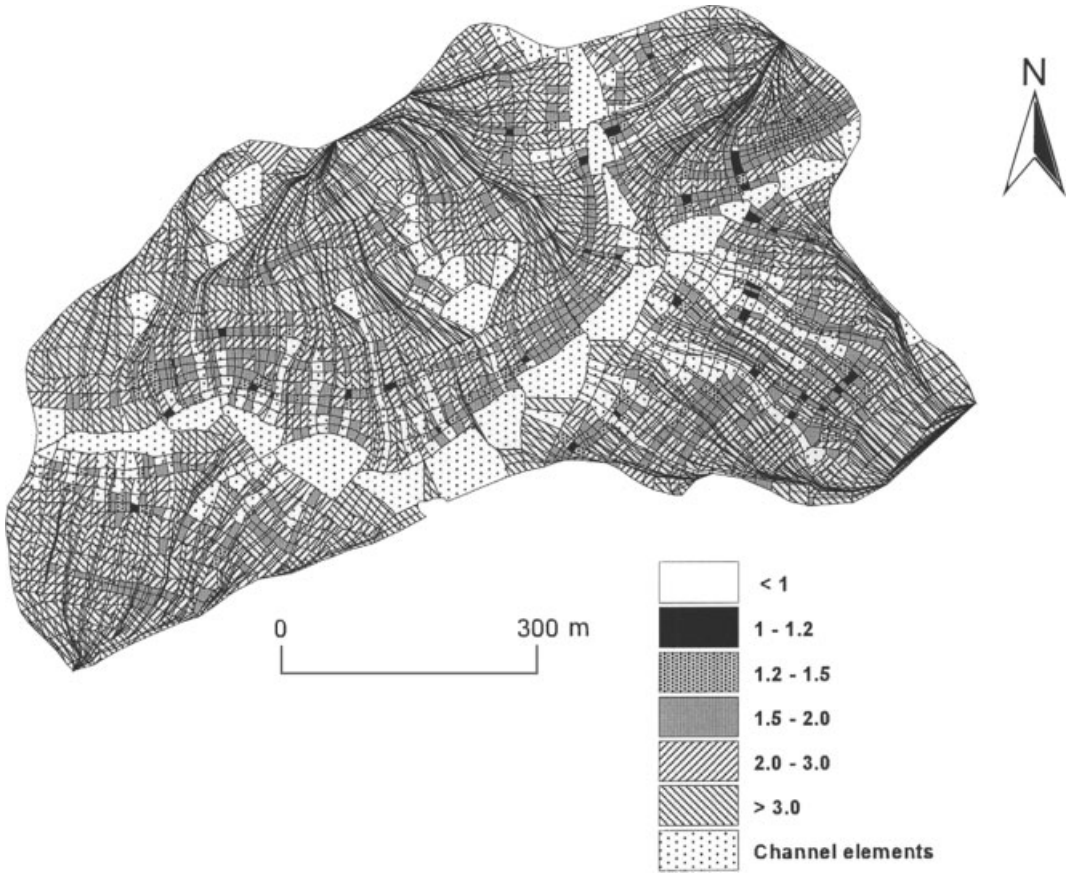

Figure 4. Spatial distribution of safety factor in the study area with the simulation of storm 67. For characteristics of storm 67 refer to Table IV and Figure 5

Table V. Failure time (TF: time at which safety factor is ≤ 1), cumulative rainfall (CR), and hourly rainfall intensity (RI) at the time of failure for six simulated unstable elements

Element ID	Rainstorm 67			Rainstorm 62			Rainstorm 45			Rainstorm 1			Rainstorm 80			Rainstorm 44		
	TF	CR	RI	TF	CR	RI	TF	CR	RI	TF	CR	RI	TF	CR	RI	TF	CR	RI
349	22	138	6·0	24	107	15·7	16	146	13·6	15	121	4·8	22	86	3·3	19	122	7·8
2779	24	159	10·7	29	185	18·4	18	175	13·8	13	112	4·7	44	255	7·3	25	173	3·6
708	30	229	13·5	34	236	6·9	24	204	4·0	30	180	4·2	47	273	4·2	29	185	1·6
533	31	243	14·0	37	250	6·2	—	—	—	—	—	—	—	—	—	—	—	—
434	34	266	6·2	39	257	2·5	—	—	—	—	—	—	—	—	—	—	—	—
559	36	277	6·4	35	239	3·2	23	200	4·0	14	116	4·8	—	—	—	—	—	—

finding is supported by results from piezometric response in unstable sites (Sidle and Swanston, 1982; Sidle 1984a; Sidle and Tsuboyama, 1992). The combination of minimum cumulative rainfall and hourly rainfall intensity required to trigger a landslide varied among different rainstorms (Table V). The minimum combined cumulative rainfall and the hourly rainfall intensity (at failure time) that triggered a landslide were 86 mm and 3·3 mm h^{-1} respectively for element 349 in storm 80 (Table V).

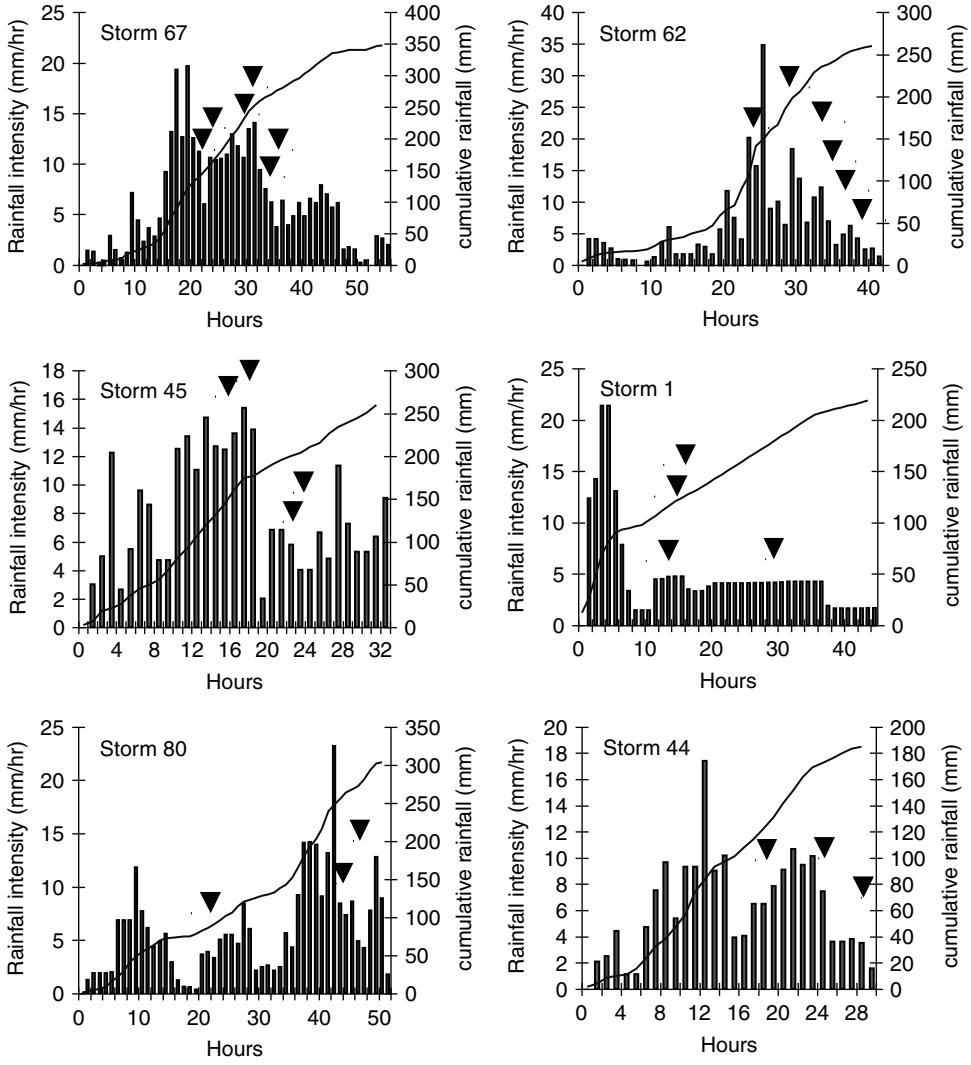

Figure 5. Hyetographs of six important rainstorms (excluding uniform rainstorms) that generated large numbers of unstable elements. The failure time for unstable elements is shown in the figure by inverted triangles

Temporal changes in safety factor for six unstable elements were simulated for storms 67, 62, and their 'uniform intensity' counterparts (storms A and B, Figure 6). The safety factor decreases gradually as the rainfall gradually builds up pore water pressure; safety factor then drops suddenly in response to critical inputs of subsurface water. In addition to rainstorm characteristics, the topographic characteristics of elements and the surrounding area controlled the rate of decrease in safety factor during the rainstorms, especially the combination of slope gradient and upslope area. Topographic characteristics for all unstable elements are shown in Table VI. Element 349, which had the steepest gradient and largest upslope area, failed earliest in all rainstorms except in storm 1 (see Table V). All unstable elements had very steep (>48°) slope gradients (Table VI). Simplified applications of the infinite slope model to low-cohesion soils have used slope gradient as the sole indicator of landslide potential (e.g. Lohnes and Handy, 1968; Carson and Petley, 1970; Swanston, 1974; Ballard and Willington, 1975). However, influences of the variability of soil properties, vegetation

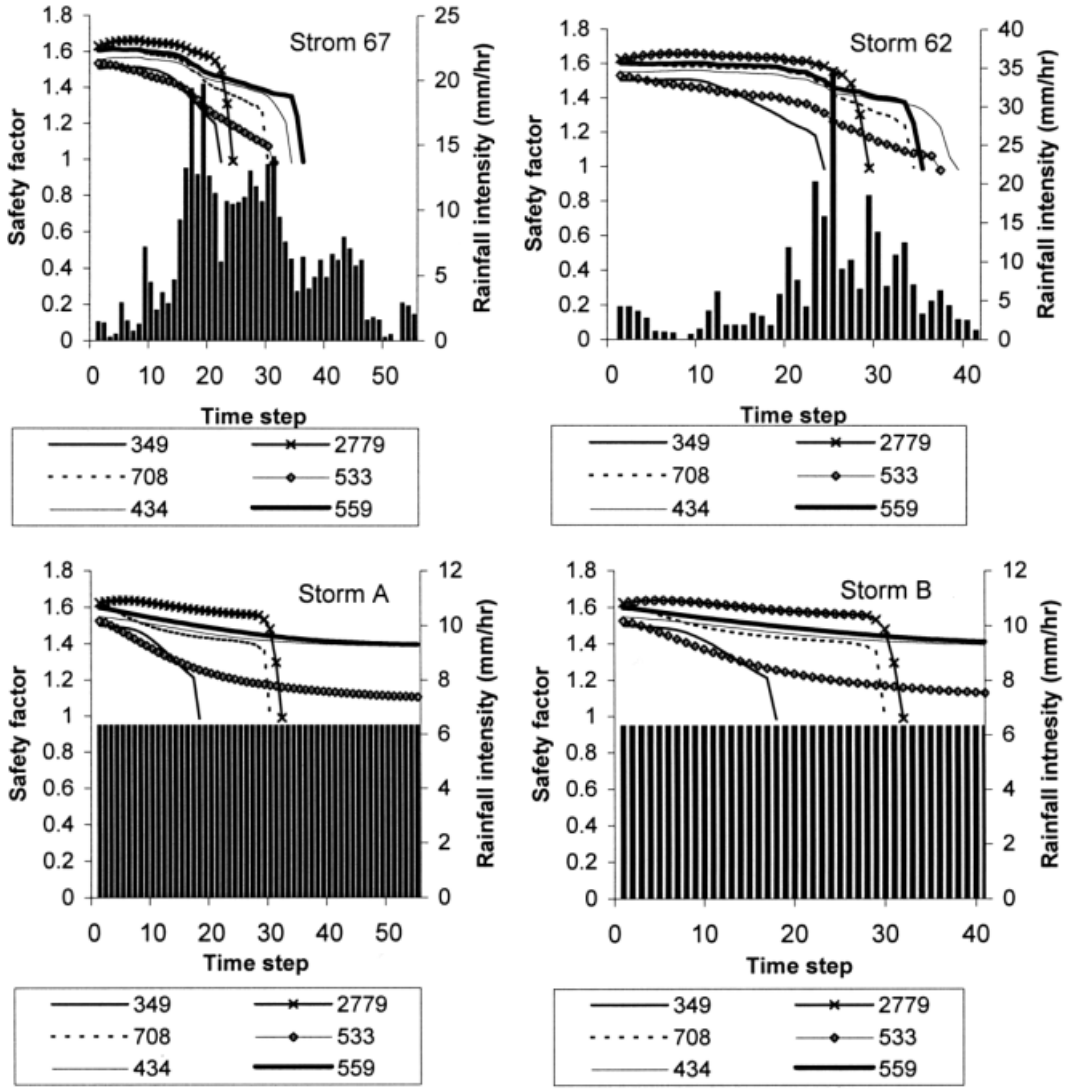

Figure 6. Temporal changes in safety factor for unstable elements when simulated with rainstorms 67, 62, and their synthetic 'uniform intensity' counterparts. Rainstorms 67 and 62 produced six unstable elements, and storms A and B produced three unstable elements

conditions, and other topographic features are important considerations. In many cases, marginally stable elements may not fail if some level of vegetation rooting strength is maintained on steep sites or if sites are not harvested (Wu and Sidle, 1995; Sidle and Wu, 1999). The unstable elements also depict relatively large upslope area. In the stream tube networks, only 12% and 27% of the total elements have upslope areas greater than 1000 m^2 and 500 m^2 respectively. The influence of upslope catchment area on groundwater response, and thus on landslide initiation, is well established (Tarboton, 1997).

Hydraulic conductivity and rainstorms

The accretion of shallow groundwater in hillslopes due to piping, preferential flow, and matrix flow has been noted by many researchers (Tsukamoto *et al*., 1982; Sidle 1984a; Tsukamoto and Ohta, 1988; Montgomery *et al*., 1997; Tsuboyama *et al*., 1994, 2000). Subsurface flow in forest soils is facilitated by an interconnected

Table VI. Topographic characteristics of unstable elements

Element ID	Upslope area (m^2)	Slope gradient (degrees)
349	1957	56·5
2779	422	49·1
708	1433	48·1
434	629	52·2
559	660	49·8
435	970	48·9

network of macropores created by roots, buried organic matter, animal burrows, and cracks between aggregates and rocks (e.g. Beven and Germann, 1982; Tsukamoto and Ohta, 1988; Noguchi *et al*., 1999; Sidle *et al*., 2001). Thus, K_{sat} used to characterize subsurface flow should be an effective K_{sat} of the soil rather than the K_{sat} of small samples of the soil matrix (Moore and Grayson, 1991). Such quantification is extremely difficult, as it encompasses large and potentially variable portions of the hillslope catena (Chappell and Ternan, 1992; Sidle *et al*., 2001).

To assess the effect of K_{sat} during rainstorms on landslide occurrence, simulations were conducted for the minimum ($K_{sat} = 2{\cdot}8 \times 10^{-4}$ m s^{-1}) and maximum ($K_{sat} = 2{\cdot}5 \times 10^{-3}$ m s^{-1}) values of hydraulic conductivity reported in the study area (Fannin *et al*., 2000). Results from these 172 simulations (86 rainstorms times two K_{sat} values) are shown in Table VII, along with results of earlier simulations that used a mean value of $K_{sat}(1{\cdot}4 \times 10^{-3}$ m $s^{-1})$. All rainstorms (except the shortest duration storms 30 and C) produced

Table VII. Results of simulations under different K_{sat} scenarios.[a] For comparison, the results of mean K_{sat} condition from Table IV are reproduced. Refer to Table IV for rainfall characteristics

Storm no.	$K_{sat} = 1{\cdot}4 \times 10^{-3}$ m s^{-1}			$K_{sat} = 2{\cdot}8 \times 10^{-4}$ m s^{-1}			$K_{sat} = 2{\cdot}5 \times 10^{-3}$ m s^{-1}		
	RS	NUE	NMSE	RS	NUE	NMSE	RS	NUE	NMSE
67	1	6	41	1	20	140	1	3	23
62	2	6	38	5	18	75	2	3	21
45	3	4	35	4	18	77	2	3	21
1	4	4	18	15	6	46	11	0	4
80	5	3	37	3	19	105	3	2	15
A	6	3	33	2	19	140	4	1	11
B	7	3	24	7	9	73	6	1	9
44	8	3	19	22	4	33	5	1	10
30	9	3	12	45	1	2	7	0	8
64	10	2	16	6	10	6	9	0	5
27	11	2	15	48	3	12	8	0	7
41	12	2	14	20	5	38	9	0	5
58	12	2	14	10	8	65	10	0	4
18	13	2	13	14	7	61	10	0	4
42	14	2	12	28	4	23	9	0	5
70	14	2	12	8	9	71	10	0	4
C	15	2	11	45	1	2	7	0	8
8	15	2	11	21	5	36	10	0	4
11	15	2	11	16	6	45	10	0	4
47	15	2	11	25	4	26	10	0	4
73	15	2	11	17	6	31	10	0	4

[a] RS: rank of the storm; NUE: number of unstable elements (safety factor ≤ 1); NMSE: number of marginally stable elements (safety factor >1 and $<1{\cdot}2$).

larger numbers of landslides with low K_{sat} values compared with the mean K_{sat} condition. Storm 67 produced the largest number of landslides in all K_{sat} simulations. During storm 67, when K_{sat} was lowered to $2{\cdot}8 \times 10^{-4}$ m s^{-1}, 20 unstable elements were simulated.

Although more unstable elements were produced for low K_{sat} conditions (compared with mean K_{sat}), the degree of importance of rainstorms that initiated landslides varied between the two K_{sat} conditions. For example, the mean K_{sat} simulations for storms 1 and 80 produced four and three unstable elements respectively; however, the low K_{sat} simulations for storm 80 (total rainfall 304 mm) and storm 1 (total rainfall 219 mm) produced 19 and six unstable elements respectively (Table VII). Similarly, landslide simulations using low K_{sat} for the longest rainstorm (storm 58; total rainfall amount 269 mm) produced eight unstable elements, whereas the shortest rainstorm (storm 30; total rainfall amount 123 mm) produced only one unstable element. For mean K_{sat} simulations, storm 30 produced more unstable elements than storm 58 (Table VII).

Landslide simulations for storms 1, 27, 42, 44, and 47 with low K_{sat} values, resulted in about a two fold increase in the number of unstable elements compared with mean K_{sat} conditions; simulations for storms 30 and C produced similar magnitudes of decreases in unstable elements. The relative ranking of all seven of these storms related to their potential to trigger landslides is greatly reduced in the low K_{sat} simulations compared with the mean K_{sat} simulations. All of these rainstorms (except storm 1) have total rainfall $<$200 mm. On the other hand, storms 80, A, 64, 58, and 70 (total rainfall $>$250 mm) produced four- to six-fold greater numbers of unstable elements during low K_{sat} simulations compared with mean K_{sat} simulations, and the ranking related to landslide initiation was higher for the low K_{sat} simulations than the mean K_{sat} simulations. These findings suggest that for low K_{sat} conditions the combined influence of all four storm factors are important considerations for landslide initiation, but that the total amount of rainfall appears to become the dominant influence.

During low K_{sat} simulations, storm 67 (total rainfall 349 mm) and storm 62 (total rainfall 260 mm) produced large numbers of unstable elements compared with their synthesized 'uniform intensity' counterpart storms, A and B respectively. Similarly, the longest storm (storm 58; total rainfall 269 mm) produced the same number of unstable elements as its synthesized 'uniform intensity' counterpart (storm D; not shown in Table VII), but they generated 65 and 56 marginally stable elements respectively. At low K_{sat} values, the shortest rainstorm (storm 30; total rainfall 123 mm) and its synthesized 'uniform intensity' counterpart (storm C) produced the same numbers of both unstable elements and marginally stable elements. Hence, for low K_{sat} scenarios, the effect of short-term rainfall intensity peaks on occurrence of landslides was more important for rainstorms with higher rainfall amounts (and high mean intensities) than for storms with lower rainfall amounts.

When K_{sat} was raised to $2{\cdot}5 \times 10^{-3}$ m s^{-1}, only six rainstorms produced unstable elements. Rainstorm 67 produced three unstable elements and 21 marginally unstable elements, the largest of all the rainstorms (Table VII). Many rainstorms did not produce unstable elements, probably due to the rapid flow of groundwater downslope and the resultant dissipation of pore water pressure. The shortest rainstorm (storm 30), however, again produced more marginally stable elements than the longest storm (storm 58). For high K_{sat} conditions, storms 67 and 62 produced more unstable elements than the synthesized 'uniform intensity' counterparts, whereas storms 30 and 58 produced equal numbers of marginally stable elements compared with their synthesized 'uniform intensity' counterparts.

When compared with results of low and mean K_{sat} simulations, it appears that only rainstorms with high mean and maximum hourly intensity, duration, and rainfall amount trigger landslides in soils with high K_{sat}. The influence of temporal patterns of short-term intensity ceased for high K_{sat} conditions, unless the total rainfall and mean and maximum hourly rainfall intensity was reasonably high. Hence, when K_{sat} is spatially variable, a more complex phenomenon of subsurface water movement may determine landslide occurrence.

Soil depth and rainstorms

Differences in the piezometric response in hillslope soils to precipitation have also been attributed to soil depth (Pierson, 1980). To evaluate the influence of soil depth on landslide occurrence, soil depth was altered

Table VIII. Results of simulations for different soil depth (D) scenarios for the mean K_{sat} condition ($K_{sat} = 1{\cdot}4 \times 10^{-3}$ m s^{-1}).[a] For comparison, results of soil depth of 1 m from Table IV are also shown. Refer to Table IV for rainstorms characteristics

Storm no.	$D = 1{\cdot}0$ m			$D = 1{\cdot}3$ m			$D = 1{\cdot}5$ m		
	RS	NUE	NMSE	RS	NUE	NMSE	RS	NUE	NMSE
67	1	6	41	1	33	28	1	37	50
62	2	6	38	4	22	27	2	31	56
45	3	4	35	3	22	28	3	25	57
1	4	4	18	11	7	10	10	11	29
80	5	3	37	2	22	30	4	24	60
A	6	3	33	5	19	26	5	24	54
B	7	3	24	6	15	25	6	12	46
44	8	3	19	17	6	11	14	8	35
30	9	3	12	7	11	16	7	12	37
64	10	2	16	14	6	14	35	5	42
27	11	2	15	8	9	13	8	11	37
41	12	2	14	9	7	12	9	11	35
58	12	2	14	13	7	8	11	11	23
18	13	2	13	12	7	9	10	11	29
42	14	2	12	10	7	11	16	8	30
70	14	2	12	20	6	8	13	10	26
C	15	2	11	22	4	15	35	5	42

[a] RS: rank of the storm; NUE: number of unstable elements (safety factor ≤ 1); NMSE: number of marginally stable elements (safety factor >1 and $<1{\cdot}2$).

to 0·5, 0·7, 1·3, and 1·5 m in each of 86 rainstorm simulations, leading to an additional 344 simulations. All these simulations use the mean K_{sat} values ($1{\cdot}4 \times 10^{-3}$ m s^{-1}). These results are summarized in Table VIII for the top 17 ranked storms that generated the largest numbers of unstable elements when using an average soil depth of 1 m. No unstable elements occurred in the shallower soil (0·5 and 0·7 m) during any rainstorms; thus, they were excluded from Table VIII. A large number of failures occurred in deeper soils (1·3 and 1·5 m). Even though the degree of importance of these rainstorms in generating landslides varied for different soil depth conditions, the scenario was complex. The interaction of soil depth in the groundwater simulations, as well as in safety factor calculations, caused this complexity. Clearly, the results from the shortest rainstorm (storm 30) and its synthetic 'uniform intensity' storm (storm C) were least influenced by increasing soil depth. Storm 30 produced three, six, and five unstable elements for soil depths of 1 m, 1·3 m and 1·5 m respectively. Hence, with increased soil depth, the shortest duration storm of high intensity caused the least increase in unstable elements. Wieczorek (1987) and Haneberg (1991) have reported unstable conditions in thin soils during short-duration rainstorms of high intensity.

CONCLUSIONS

Landslide occurrence during rainstorms with different characteristics (i.e. storm mean and maximum hourly intensity, duration, and rainfall amount) was examined in 602 simulations using an IDSSM designed to analyse rapid, shallow landslides. The effects of K_{sat} and soil depth for different rainstorms were also examined for a sub-watershed in Carnation Creek, located on Vancouver Island, British Columbia, Canada. The soil and vegetation parameters were treated as constants in the study area because of limited information. The major findings from this series of distributed simulations are as follows.

1. The number of landslides produced by different rainstorms and the degree of importance of rainstorms in producing landslides depended on the combined influence of mean and maximum hourly intensity, duration, and total rainfall amount. The temporal distribution of short-term intensity also affected landslide occurrence. The number of landslides produced by different rainstorms and their degree of importance depended on site characteristics such as K_{sat} and soil depth.
2. The same rainstorm influenced landslide initiation differently depending on site characteristics. In general, low values of K_{sat} produced more landslides and higher values generated fewer landslides in all rainstorms. Similarly, deeper soils had more landslides than thinner soils in all rainstorms. The shortest and the longest rainstorms were highly influenced by changes in the soil properties.
3. For low K_{sat} simulations, total rainfall appeared to have a greater influence on landslide occurrence. For mean K_{sat} conditions, in addition to all four characteristics of rainstorms, the temporal distribution of rain intensity affected landsliding. During high K_{sat} simulations, only six rainstorms with high mean and maximum hourly intensity, duration and total rainfall amount generated landslides.
4. Usually, actual rainstorms produced larger numbers of unstable elements than their synthetic 'uniform intensity' counterparts, indicating the importance of short-term rainfall intensity peaks in triggering landslides. Although the shortest duration rainstorm and its synthetic 'uniform intensity' counterpart produced equal numbers of unstable/marginally stable elements for low K_{sat} and deep soil simulations, none of the synthetic 'uniform intensity' rainstorms produced more unstable conditions than their real rainstorm counterparts in any simulation.
5. In addition to rainstorm characteristics, the topographic characteristics of elements and the surrounding area controlled landslide occurrence and the time of failure. All unstable elements occurred on very steep slopes.
6. In all rainstorms, most failures occurred after some threshold of cumulative rainfall and maximum hourly rainfall intensity. The safety factor decreased gradually as rainfall slowly built up pore water pressure; safety factor then dropped suddenly in response to critical inputs of subsurface water.

The IDSSM is arguably the most sophisticated, physically based landslide model available. The results of this study confirm the results from similar field investigations. The model has great versatility in computing the relative influences of different rainstorms on landslide occurrence. It has clearly been shown that the same rainstorm may influence landsliding differently depending on the site characteristics. Hence, any threshold criteria, such as between mean intensity and mean duration, that is developed to assess the occurrence of landslides should be recognized to be site specific. Studies based on field investigations confirm this finding. For example, Wieczorek (1987) found that landslides occurred after continuous high-intensity rainfall in a 10 km^2 area near La Honda, California, whereas Kay and Chen (1995) report landslides in Hong Kong following a combination of high hourly and daily rainfall. Our study also indicated that the combined influence of different characteristics of rainstorms and the short-term hourly rainfall intensity peaks are important for landslide occurrence. Because this type of detailed analysis requires spatially distributed field data, we were typically hindered by unavailability of such detailed site parameters and rainstorm–landslide data. Therefore, this modelling study is a first attempt to develop insights into the distributed behaviour of landsliding during large rainstorms with varying characteristics at the basin scale.

ACKNOWLEDGEMENTS

The study was supported by British Columbia Advanced System Institute under the Forestry Innovation Development Program. This project has been partially funded by Forest Renewal British Columbia (FRBC). It is acknowledged that Amod S. Dhakal had won the Killam Postdoctoral award administered by Izaak Walton Killam Memorial Fund for Advanced Studies, University of British Columbia. We would like to thank Wu Weimin and Dan Hogan for their contributions at different stages of the study.

REFERENCES

Agriculture Canada Expert Committee on Soil Survey. 1987. *The Canadian system of soil classification*. Research Branch, Agriculture Canada.

Ballard TM, Willington RP. 1975. Slope instability in relation to timber harvesting in the Chilliwack Provincial Forest. *Forestry Chronicle* **51**: 59–62.

Band LE. 1986. Topographic partition of watersheds with digital elevation model. *Water Resources Research* **22**(1): 15–24.

Beven K, Germann P. 1982. Macropores and water flow in soils. *Water Resources Research* **18**: 1311–1325.

Bhandari RK, Virajh Dias AA. 1995. Rain triggered slope movements as indicators of landslide dynamics. In *Landslide*, Senneset K (ed.). Balkema: Rotterdam; 1515–1520.

Caine N. 1980. Rainfall intensity–duration control of shallow landslides and debris flows. *Geografiska Annaler Series A: Physical Geography* **62**: 23–27.

Cannon SH, Ellen SD. 1985. Rainfall conditions for abundant debris avalanches, San Francisco Bay region, California. *California Geology* **38**: 267–272.

Canuti P, Focardi P, Garzonio CA. 1985. Correlation between rainfall and landslides. *Bulletin of the International Association of Engineering Geology* **32**: 49–54.

Carson MA, Kirkby, MJ. 1972. *Hillslope Form & Processes*. Cambridge University Press: London.

Carson MA, Petley DJ. 1970. The existence of threshold hillslopes in the denudation of the landscape. *Transactions of the Institute of British Geographers* **49**: 71–95.

Capecchi F, Focardi, P. 1988. Rainfall and landslides: research into a critical precipitation coefficient in an area of Italy. In *Proceedings of the 5th International Symposium on Landslides*, Lausanne, vol. **2**; 1031–1136.

Chappell NA, Ternan JL. 1992. Flow path dimensionality and hydrological modelling. *Hydrological Processes* **6**: 327–345.

Church C, Miles, M. 1987. Meteorological antecedents to debris flow in southwestern British Columbia; some cases studies. *Reviews in Engineering Geology* **VII**: 63–79.

Croft AR, Marston RB. 1950. Summer rainfall characteristics in northern Utah. *Transactions, American Geophysical Union* **31**: 83–95.

Dhakal AS, 1995. Disaster of 1993 experienced by Nepal. In *Proceedings of the International Sabo Symposium*, Tokyo; 115–122.

Dhakal AS, Sidle RC. 2003. Long-term modelling of landslides for different forest management practices. *Earth Surface Processes and Landforms* **28**: 853–868.

D'Orsi R, D'Avila C, Ortigao JAR, Dias A, Moraes L, Santos MD. 1997. Rio-Watch: the Rio de Janeiro landslide watch system. In *Proceedings of the 2nd PSL Pan-AM Symposium on Landslides*, Rio de Janerio, vol. **1**; 21–30.

Dunne T. 1978. Field studies of hillslope processes. In *Hillslope Hydrology*, Kirkby MJ (ed.). John Wiley: New York; 227–293.

Eastwood GEP. 1975. Southwest British Columbia, southern Vancouver Island: Carnation Creek. In *Geological fieldwork: a summary of field activities of the geological division, mineral resources branch*. B. C. Department of Mines and Petroleum Resources, Government of British Columbia; 35–40.

Ekanayake JC, Phillips CJ. 1999. A model for determining thresholds for initiation of shallow landslides under near-saturated conditions in the East Coast region, New Zealand. *Journal of Hydrology (New Zealand)* **38**: 1–28.

Fannin RJ, Jaakkola J, Wilkinson JMT, Hetherington ED. 2000. The hydrologic response of soils to precipitation at Carnation Creek, British Columbia. *Water Resources Research* **36**(6): 1481–1494.

Finlay PJ, Fell R, Meguire PK. 1997. The relationship between the probability of landslide occurrence and rainfall. *Canadian Geotechnical Journal* **34**: 811–824.

Fuller G. 1977. Geology of Vancouver Island—east half. Geological Survey of Canada, *Open file 463*. Scale 1 : 250 000.

Graeme I. 1985. *Analysis of a small debris slide on coastal Vancouver Island*. BS thesis, Faculty of Forestry, University of British Columbia, Canada.

Grayson RB, Moore ID, McMahon TA. 1992. Physically based hydrologic modeling 1, a terrain-based model for investigative purposes. *Water Resources Research* **28**(10): 2639–2658.

Haneberg WC. 1991. Pore pressure diffusion and the hydrologic response of nearly saturated, thin landslide deposits to rainfall. *Journal of Geology* **99**: 886–892.

Hartman GF, Scrivener JC. 1990. Impacts of forestry practices on a coastal stream ecosystem, Carnation Creek, British Columbia. *Canadian Bulletin of Fisheries and Aquatic Sciences 223*, Department of Fisheries and Oceans, Biological Sciences Branch, Pacific Biological Station, Ottawa, Ont.

Haruyama M. 1974. Features of slope-movements due to heavy rainfalls in the Shirasu region of southern Kyushu. *Memoirs of the Faculty of Agriculture (Kagoshima University)* **10**(19): 151–163.

Hetherington E. 1982. Effects of forest harvesting on the hydrologic regime of Carnation Creek experimental watershed: a preliminary assessment. In *Proceedings, Canadian Hydrology Symposium*, National Resources Council of Canada, Fredericton, New Brunswick, 14–16 June; 247–267.

Hetherington E. 1998. Watershed hydrology. In *Carnation Creek and Queen Charlotte Islands Fish/Forestry Workshop: Applying 20 Years of Coastal Research to Management Solutions*, Hogan DL, Tschaplinski PJ, Chatwin S (eds). Ministry of Forests, Research Branch, Victoria, B.C., Canada, Land Management Handbook No. 41; 33–40.

Jackson CR, Cundy TW. 1992. A model of transient, topographically driven, saturated subsurface flow. *Water Resources Research* **28**(5): 1417–1427.

Jackson RJ. 1966. Slips in relation to rainfall and soil characteristics. *Journal of Hydrology (New Zealand)* **5**: 45–53.

Johnson KA, Sitar N. 1990. Hydrologic conditions leading to debris flow initiation. *Canadian Geotechnical Journal* **27**: 789–801.

Kay JN, Chen, T. 1995. Rainfall–landslide relationship for Hong Kong. In *Proceedings, The Institution of Civil Engineers Geotechnical Engineering* **113**: 117–118.

Keefer DK, Wilson RC, Mark RK, Brabb EE, Brown WM, Ellen SD, Harp EL, Wieczorek GF, Alger CS, Zatkin RS. 1987. Real-time landslide warning during heavy rainfall. *Science* **238**: 921–925.

Kim SK, Hong WP, Kim YM. 1992. Prediction of rainfall-triggered landslides in Korea. In *Proceedings of the 6th International Symposium on Landslides*, vol. 2. Bell DH (ed.). Balkema: 989–994.
Krajina VJ. 1969. Ecology of forest trees in British Columbia. In *Ecology of Western North America*, Krajina VJ, Brooke RC (eds). Department of Botany, University of British Columbia: Vancouver; 1–146.
Larsen MC, Simon A. 1993. A rainfall intensity–duration threshold for landslides in a humid-tropical environment, Puerto Rico. *Geografiska Annaler Series A: Physical Geography* **75**: 13–23.
Lohnes RA, Handy RL. 1968. Slope angles in friable loess. *Journal of Geology* **76**(3): 247–258.
Ministry of Forests. 1991. *Topographic and drainage system map of Carnation Creek watershed* (1 : 5000). Research Branch, Ministry of Forests British Columbia, 1 sheet.
Montgomery DR, Dietrich, WE. 1988. Where do channels begin? *Nature* **336**(17): 232–234.
Montgomery DR, Dietrich WE. 1994. A physically based model for the topographic control on shallow landsliding. *Water Resources Research* **30**: 1153–1171.
Montgomery DR, Dietrich WE, Torres R, Anderson SP, Heffner JT, Loague K. 1997. Hydrologic response of a steep, unchanneled valley to natural and applied rainfall. *Water Resources Research* **33**: 91–109.
Moore ID, Burch GJ. 1986. Sediment transport capacity of sheet and rill flow: application of unit stream power theory. *Water Resources Research* **22**(8): 1350–1360.
Moore ID, Grayson RB. 1991. Terrain-based catchment partitioning and runoff prediction using vector elevation data. *Water Resources Research* **27**(6): 117–1191.
Moore ID, O'Loughlin EM, Burch GJ. 1988. A contour based topographic model and its hydrologic and ecological applications. *Earth Surface Processes and Landforms* **13**: 305–320.
Noguchi S, Tsuboyama Y, Sidle RC, Hosoda I. 1999. Morphological characteristics of macropores and distribution of preferential flow pathways in a forested slope segment. *Soil Science Society of America Journal* **63**(5): 1413–1423.
O'Loughlin CL, Rowe LK, Pearce AJ. 1982. Exceptional storm influences on slope erosion and sediment yields in small forest catchments, North Westland, New Zealand. *National Conference Publication 82/6*, Institute of Engineering, Barton, ACT, Australia; 84–91.
Onda Y, Mori A, Shindo S. 1992. The effects of topographic convergence and location of past landslides on subsurface water movement on granite hillslope. *Journal of Natural Disaster Science* **14**: 45–58.
Oswald ED. 1974. Vegetation and soils of Carnation Creek watershed (upper section). *Report BC-P-11-74*, Canadian Forestry Service, Pacific Forest Research Centre, Victoria, B.C.
Pierson TC. 1980. Piezometric response to rainstorms in forested hillslope drainage depressions. *Journal of Hydrology* **19**: 1–10.
Pierson TC. 1983. Soil pipes and slope stability. *Quarterly Journal of Engineering Geology* **16**: 1–11.
Selby MJ. 1976. Slope erosion due to extreme rainfall: a case study from New Zealand. *Geografiska Annaler Series A: Physical Geography* **58**: 131–138.
Schroeder WL, Alto JV. 1983. Soil properties for slope stability analysis: Oregon and Washington coastal mountains. *Forest Science* **29**(4): 823–833.
Sidle RC. 1984a. Shallow groundwater fluctuations in unstable hillslopes of coastal Alaska. *Zertschrift für Gletscherkunde und Glazialgeologie* **20**: 79–95.
Sidle RC. 1984b. Relative importance of factors influencing landsliding in coastal Alaska. In *Proceedings, 21st Annual Engineering Geology and Soils Engineering Symposium*, University of Idaho, Moscow, ID; 311–325.
Sidle RC. 1986. Groundwater accretion in unstable hillslopes of coastal Alaska. In *Conjunctive Water Use*, Goreluck SM (ed.). IAHS Publication no. 156. IAHS Press: Wallingford; 335–343.
Sidle RC. 1991. A conceptual model of changes in root cohesion in response to vegetation management. *Journal of Environmental Quality* **20**: 43–52.
Sidle RC. 1992. A theoretical model of the effects of timber harvesting on slope stability. *Water Resources Research* **28**: 1897–1910.
Sidle RC, Swanston DN. 1982. Analysis of a small debris slide in coastal Alaska. *Canadian Geotechnical Journal* **19**: 167–174.
Sidle RC, Tsuboyama Y. 1992. A comparison of piezometric response in unchanneled hillslope hollows: coastal Alaska and Japan. *Journal of Japan Society of Hydrology & Water Resources* **5**: 3–11.
Sidle RC, Wu W. 1999. Simulating effects of timber harvesting on the temporal and spatial distribution of shallow landslides. *Zertschrift für Geomorphologie, N F* **43**(2): 185–201.
Sidle RC, Pearce AJ, O'Loughlin CL. 1985. *Hillslope Stability and Land Use*. American Geophysical Union, Water Resources Monograph. AGU: Washington, DC.
Sidle RC, Noguchi S, Tsuboyama Y, Laursen K. 2001. A conceptual model of preferential flow systems in forested hillslopes: evidence of self-organization. *Hydrological Processes* **15**: 1675–1692.
Smith AA. 1980. A generalized approach to kinematic flood routing. *Journal of Hydrology* **45**: 71–89.
Swanston DN. 1974. The slope stability problems associated with timber harvesting in mountainous regions of the western United States. *US Department of Agriculture Forest Service Technical Report PNW-21*. Pacific Northwest Forest and Range Experiment Station: Portland, Oregon.
Takasao T, Shiiba M. 1988. Incorporation of the effect of concentration of flow into the kinematic wave equations and its applications to runoff system lumping. *Journal of Hydrology* **102**: 301–322.
Tarboton D. 1997. A new method for the determination of flow directions and upslope areas in grid digital elevation models. *Water Resources Research* **33**(2): 309–319.
Tsuboyama Y, Hosoda I, Noguchi S, Sidle RC. 1994. Piezometric response in a zero-order basin, Hitachi Ohta, Japan. In *Proceedings of International Symposium on Forest Hydrology*, Ohta T (ed.), University of Tokyo, Japan; 217–224.
Tsuboyama Y, Sidle RC, Noguchi S, Murakami S, Shimizu T. 2000. A zero-order basin—its contribution to catchment hydrology and internal hydrological processes. *Hydrological Processes* **14**: 387–401.
Tsukamoto Y, Ohta T. 1988. Runoff processes on a steep forested slope. *Journal of Hydrology* **102**: 165–178.

Tsukamoto Y, Ohta T, Noguchi H. 1982. Hydrological and geomorphological studies of debris slides on forested hillslopes in Japan. In *Recent Developments in the Explanation and Prediction of Erosion and Sediment Yield*, Walling DE (ed.). IAHS–AISH Publication 137. IAHS Press: Wallingford; 89–98.

Wieczorek GF. 1987. Effect of rainfall intensity and duration on debris flows in central Santa Cruz Mountains, California. *Reviews in Engineering Geology* **VII**: 93–104.

Wieczorek GF. 1996. Landslide triggering mechanisms. In *Landslides: investigation and mitigation*, Turner AK, Schuster RL (eds). Transportation Research Board, Special Report 247, Washington, DC; 76–90.

Wilson RC. 1997. Normalizing rainfall/debris-flow thresholds along the U.S. Pacific Coast for long-term variations in precipitation climate. In *Proceedings, 1st International Conference On Debris-Flow Hazards Mitigation: Mechanics, Prediction and Assessment*, Chen C-L (ed.). American Society of Civil Engineers: San Francisco; 32–43.

Wu W, Sidle RC. 1995. A distributed slope stability model for steep forested hillslopes. *Water Resources Research* **31**: 2097–2110.

Ziemer RR, Lewis TE, Rice RM, Lisle TE. 1991. Modeling the cumulative watershed effects of forest management strategies. *Journal of Environmental Quality* **20**: 36–42.

